Research Square

Preprints are preliminary reports that have not undergone peer review.
They should not be considered conclusive, used to inform clinical practice,
or referenced by the media as validated information.

# Electron diffraction determines crystal structures from all ten acalabrutinib samples spanning anhydrates, hydrates, and solvates

**Alex Chen**

alex_chen@crystalpharmatech.com

Crystal Pharmatech Inc.

**Yuhao Chen**

Crystal Pharmatech Co., Ltd.

**Gustavo Santiso-Quinones**

Eldico Scientific AG

**Yuwen Xu**

Crystal Pharmatech Co., Ltd.

**Yingjie Li**

Crystal Pharmatech Co., Ltd.

**Chunxiang Huang**

Crystal Pharmatech Co., Ltd.

**Jiale Qian**

Crystal Pharmatech Co., Ltd.

**Gunther Steinfeld**

Eldico Scientific AG

**Christian Jandl**

Eldico Scientific AG

**Johannes Merkelbach**

Eldico Scientific AG

**Hailu Zhang**

Institute of Frontier Solid-State Chemistry, Crystal Pharmatech Co., Ltd.

**Liping Meng**

Crystal Pharmatech Co., Ltd.

**Robert Wenslow**

Crystal Pharmatech Inc.

---

**Article**

**Keywords:**

**Posted Date:** November 13th, 2026

**DOI:** https://doi.org/10.21203/rs.3.rs-11694963/v1

**License:** This work is licensed under a Creative Commons Attribution 4.0 International License.
Read Full License

**Additional Declarations:** Competing interest reported. G.S.-Q., G.S., C.J. and J.M. are employees of Eldico Scientific AG, which manufactures and commercializes the ELDICO ED-1 electron diffractometer used in this study; G.S.-Q. and G.S. are founders and shareholders of the company. Y.C., Y.X., Y.L., C.H., J.Q., L.M., R.W. and A.M.C. are employees of Crystal Pharmatech. H.Z. serves as Dean of the Institute of Frontier Solid-State Chemistry at Crystal Pharmatech. Crystal Pharmatech commercially provides pharmaceutical solid-state research services, including polymorph screening, solid-form characterization and ED-based crystal-structure determination; R.W. and A.M.C. are co-founders and shareholders of Crystal Pharmatech. This study was funded by Crystal Pharmatech and Eldico Scientific AG.

# Electron diffraction determines crystal structures from all ten acalabrutinib samples spanning anhydrates, hydrates, and solvates

Yuhao Chen[1], Gustavo Santiso-Quinones[2*], Yuwen Xu[1], Yingjie Li[1], Chunxiang Huang[1], Jiale Qian[1], Gunther Steinfeld[2], Christian Jandl[2], Johannes Merkelbach[2], Hailu Zhang[3], Liping Meng[1], Robert Wenslow[4], Alex M. Chen[1,3,4*]

[1] Crystal Pharmatech Co., Ltd., 288 Jiangyun Road, Suzhou Industrial Park, Suzhou, China, 215123.

[2] Eldico Scientific AG, Hegenheimermattweg 167a, Allschwil, Switzerland.

[3] Institute of Frontier Solid-State Chemistry, Crystal Pharmatech Co., Ltd., 288 Jiangyun Road, Suzhou Industrial Park, Suzhou, China, 215123.

[4] Crystal Pharmatech Inc., Suite 500-B, 3000 Eastpark Blvd, Cranbury, NJ, 08512.

[*] Corresponding authors: santiso@eldico.ch; alex_chen@crystalpharmatech.com.

# 1. Abstract

Microcrystal electron diffraction can determine crystal structures from pharmaceutical powders, but its performance across a diverse set of routine-origin solid forms from one highly polymorphic compound has not been systematically evaluated. We evaluated ten acalabrutinib forms selected from more than thirty identified forms and spanning anhydrates, hydrates, and solvates. Samples came from routine screening, preparation, or scale-up without purpose-grown single crystals or morphology optimization; selection was independent of apparent crystallinity, morphology, and anticipated diffraction quality. Electron diffraction determined crystal structures from all ten crystalline powder samples. Nine corresponded to selected forms, while one yielded a different form following solid-form conversion. Mother-liquor preservation combined with cryogenic preparation most consistently enabled determination of labile hydrate and solvate structures. Integration with conventional characterization detected conversions and resolved ambiguous solvent and water contents. Here, we establish a systematic single-compound benchmark supporting direct crystal-structure determination from diverse pharmaceutical crystalline powders in routine solid-form workflows.

## 2. Introduction

Polymorphism remains one of the most consequential and challenging phenomena in pharmaceutical solid-state science. Different crystalline forms of a drug substance can exhibit markedly distinct physicochemical properties, including solubility, dissolution rate, chemical and physical stability, and mechanical properties, with direct implications for bioavailability, manufacturability, and regulatory approval.[1–3] As a result, unambiguous structural identification of polymorphs is not merely an academic exercise but an increasingly important scientific and regulatory objective. Regulatory guidelines, including ICH Q6A and FDA guidance on pharmaceutical solid polymorphism, emphasize solid-form characterization and polymorph control in Chemistry, Manufacturing and Controls (CMC) submissions, underscoring the importance of reliable, structurally informative methods throughout drug development.[4,5]

Despite these requirements, definitive crystal structure determination for pharmaceutical solids is frequently hindered because many solid forms are obtained as crystalline powders and do not readily yield single crystals suitable for single-crystal X-ray diffraction (SC-XRD).[6–8] In practice, polymorph identification therefore relies heavily on a combination of indirect techniques such as X-ray powder diffraction (XRPD), thermal analysis, and spectroscopy.[9] While powerful, these approaches may not definitively establish solid-form identity, including whether a material is an anhydrate, hydrate, or solvate, or distinguish among different hydrate or solvate stoichiometries. Consequently, assignments based solely on such data may remain ambiguous and, in complex systems, can be misleading.[10,11]

Electron diffraction (ED), particularly its continuous-rotation three-dimensional implementation (3D ED), commonly termed microcrystal electron diffraction (MicroED), has recently emerged as a transformative approach for crystal structure determination from crystalline powders that do not yield single crystals suitable for SC-XRD.[12,13] By leveraging the strong interaction between electrons and matter, ED enables the acquisition of diffraction data from crystals several orders of

magnitude smaller than those required for X-ray-based methods. This capability directly addresses a central bottleneck in pharmaceutical crystallography.[14] The availability of purpose-built electron diffractometers specifically engineered for chemical crystallography has substantially lowered the barrier to routine implementation of ED across both academic and industrial settings.[15] Regulatory recognition has begun to follow: The Technical Guideline for the Study of Polymorphism of Innovative Chemical Drugs (For Trial Implementation), issued by the Center for Drug Evaluation of China's National Medical Products Administration in January 2026, lists microcrystal electron diffraction (MicroED) among the techniques used for solid-form characterization, alongside SC-XRD, XRPD, vibrational spectroscopy, thermal analysis, and solid-state NMR.[16]

ED has demonstrated utility in pharmaceutical small-molecule structure determination through individual applications and broader assessments of the method.[17–22] However, its performance across a comparatively large and diverse set of routine-origin solid forms from a single highly polymorphic API has not been systematically evaluated.

Acalabrutinib is a BTK inhibitor approved for B-cell malignancies.[23,24] It was selected as a model compound because of its rich solid-form landscape. More than 1,000 crystallization experiments identified over thirty distinct solid forms based on XRPD patterns and supporting solid-state characterization data. Ten forms were selected to encompass anhydrates, hydrates, and solvates. Eight were selected based on stock availability, and two additional forms were re-prepared to bring the set to ten. Within these design constraints, the forms were not selected based on apparent crystallinity, crystal dimensions, morphology, or anticipated diffraction quality. All samples originated from routine polymorph screening, or routine re-preparation or scale-up of screening hits. No experiments specifically targeted single-crystal growth, crystal-morphology optimization, or ED suitability.

Samples were evaluated as vacuum-dried solids, room-temperature air-dried solids, or mother-liquor suspensions, using either room-temperature or cryogenic grid preparation and transfer. In

both procedures, samples were loaded onto the grid at room temperature. For cryogenic preparation, the loaded grid was plunge-cooled before cryogenic transfer; for room-temperature preparation, it was transferred without plunge cooling and cooled inside the diffractometer. All final datasets were collected at 123(2) K. These combinations allowed us to assess how sample preparation and handling affected diffraction quality, structural refinement, and preservation of the intended solid form.

Using the ELDICO *ED-1* dedicated electron diffractometer, ED successfully determined crystal structures from all ten submitted samples. Nine structures corresponded to the nine selected solid forms, whereas the sample submitted as Form K1, provisionally assigned as a tetrahydrate, yielded Form II, identified as a trihydrate, following solid-form conversion. Among the approaches evaluated, mother-liquor preservation combined with cryogenic preparation most consistently supported structure determination and more complete guest-molecule refinement for labile hydrates and solvates. The ten-of-ten structure-determination result across anhydrates, hydrates, and solvates supports incorporating ED into routine pharmaceutical solid-form workflows. The Form K1 result also demonstrates the continuing importance of conventional characterization for verifying sample identity and detecting solid-form conversions.

# 3. Results and discussion

## 3.1 Polymorph landscape overview

An extensive polymorph-screening campaign was conducted to map the solid-form landscape of acalabrutinib. Diverse crystallization strategies were employed, including solvent evaporation, cooling crystallization, antisolvent addition, reverse antisolvent addition, and salt formation followed by dissociation. Across three screening rounds, more than 1,000 experiments were performed, leading to the identification of more than 30 solid forms (Table 1) on the basis of distinct XRPD patterns, supported by complementary solid-state characterization.

**Table 1 | acalabrutinib solid-form landscape identified by polymorph screening.**

| Name | Preliminary Identification | Name | Preliminary Identification |
|---|---|---|---|
| Form I | Anhydrate | Form CS15 | (R)-1,2-Propanediol solvate |
| Form II | Trihydrate | Type A | Ethyl L-lactate solvate |
| Form III | Dihydrate | Type B | Ethylene glycol solvate |
| Form IV | Anhydrate | Type C | Poor crystallinity |
| Form V | Anhydrate | Type D | Glycerol solvate |
| Form VI | MeOH solvate | Type E | 1,2-Propanediol solvate |
| Form VII | MeOH solvate | Type F | (S)-1,2-Propanediol solvate |
| Form VIII | Acetic acid solvate | Type G | (R)-1,2-Propanediol solvate |
| Form CS6 | Anhydrate | Type H | ACN solvate |
| Form CS7 | Hydrate | Type I | Poor crystallinity |
| Form CS8 | Poor crystallinity | Type J | Anisole solvate |
| Form CS10 | IPAc solvate | Type K | Nitromethane solvate |
| Form CS11 | Hydrate | Type L | Dimethyl carbonate solvate |

| Name | Preliminary Identification | Name | Preliminary Identification |
|---|---|---|---|
| Form CS12 | Toluene solvate | Type M | Isobutanol solvate |
| Form CS13 | Hydrate | Form K1 | Hydrate (provisional tetrahydrate assignment) |
| Form CS14 | Acetylacetone solvate | Form K3 | Acetonitrile solvate |

These forms span a broad range of structural classes, including anhydrates, hydrates, and diverse solvates, such as methanol, acetic acid, ethyl lactate, glycerol, and acetonitrile solvates. The high prevalence of solvated forms highlights the strong propensity of acalabrutinib to incorporate solvent molecules into its crystal lattice, reflecting a highly adaptable and structurally diverse solid-state landscape. All previously reported polymorphs disclosed in US Patent 9,796,721 B2 (Forms I to VIII) were successfully reproduced,[24] validating the robustness of the screening approach while significantly expanding the known polymorphic space.

This pronounced structural diversity, together with the limited availability of single crystals suitable for SC-XRD, presents substantial challenges for definitive crystal structure determination by conventional solid-state characterization techniques. This motivates the central objective of the study: to benchmark ED structure-determination performance across a comparatively large and diverse set of pharmaceutical solid forms obtained through routine screening and subsequent preparation, without dedicated single-crystal growth or morphology optimization.

## 3.2 Conventional solid-state characterization

To evaluate ED performance across a comparatively large and diverse set for a single compound, ten solid forms were selected from this polymorphic landscape and subjected to further characterization. Eight were selected initially based on the availability of existing stock, and two additional forms were selected and re-prepared to bring the set to ten. The set deliberately included anhydrates, hydrates, and solvates, but the individual forms were not selected according

to apparent crystallinity, morphology, or anticipated diffraction quality. These ten selected solid forms were first analyzed using conventional solid-state characterization techniques, including XRPD, Thermogravimetric Analysis (TGA), Differential Scanning Calorimetry (DSC), and $^{1}$H NMR Spectroscopy. The corresponding data and preliminary form assignments are summarized in Table 2.

**Table 2 | Conventional solid-state characterization data for the ten forms selected for ED evaluation.**

| Forms | TGA weight loss | DSC signals (peak temp.) | Preliminary identification based on TGA and $^{1}$H NMR |
|---|---|---|---|
| **Form I** | 0.51% up to 150 °C | an endothermic peak at 209.2 °C | **Anhydrate** |
| **Form II** | 10.62% up to 90 °C | an endothermic peak at 118.0 °C | **Trihydrate** (theoretical water content of a trihydrate is 10.4%) |
| **Form III** | 7.47% up to 115 °C | an endothermic peak at 140.1 °C | **Dihydrate** (theoretical water content of a dihydrate is 7.2%) |
| **Form K1** | 15.68% up to 100 °C | three endothermic peaks at 77.1 °C, 103.4 °C and 136.7 °C; an exothermic peak at 85.9 °C | **Provisional tetrahydrate assignment** (TGA: approximately 4.8 equivalents of water; DVS: approximately 4.1 equivalents of water at 20% RH) |
| **Form K3** | 1.92% up to 120 °C, and 2.80% from 120 °C to 175 °C | three endothermic peaks at 79.0 °C, 128.5 °C and 168.7 °C | **Acetonitrile solvate** ($^{1}$H NMR signal corresponds to 0.36 equivalents of acetonitrile; TGA weight loss corresponds to ~0.23 and ~0.33 equivalents of acetonitrile for the two steps) |
| **Form CS14** | 15.72% up to 160 °C | an endothermic peak at 148.8 °C | **Acetylacetone solvate** ($^{1}$H NMR signal corresponds to 1.0 equivalents of acetylacetone; TGA weight loss corresponds to 0.87 equivalents of acetylacetone) |
| **Type A** | 1.45% up to 100 °C, and 19.45% from 100 °C to 170 °C | three endothermic peaks at 140.2 °C, 151.1 °C, and 212.5 °C and an exothermic peak at 142.1 °C | **Mono-ethyl L-lactate solvate** ($^{1}$H NMR signal corresponds to 0.95 equivalents of ethyl L-lactate; TGA weight loss corresponds to 0.97 equivalents of ethyl L-lactate) |
| **Type H** | 4.31% up to 70 °C, and 2.66% from 70 °C to 135 °C | two endothermic peaks at 106.4 °C and 135.4 °C | **Uncertain** (TGA weight loss corresponds to ~0.52 and ~0.33 equivalents of acetonitrile for the two steps. A solid-form conversion occurred during storage.) |

| Forms | TGA weight loss | DSC signals (peak temp.) | Preliminary identification based on TGA and $^1$H NMR |
|---|---|---|---|
| **Type D** | 1.07% up to 110 °C, and 4.53% from 110 °C to 165 °C | an endothermic peak at 143.9 °C and an exothermic peak at 152.4 °C | **Glycerol solvate** ($^1$H NMR signal corresponds to 1.01 equivalents of glycerol; TGA weight loss corresponds to 0.24 equivalents of glycerol) |
| **Type F** | 0.69% up to 100 °C, and 7.23% from 100 °C to 160 °C | an endothermic peak at 142.2 °C | **(S)-1,2-Propanediol solvate** ($^1$H NMR signal corresponds to 0.88 equivalents of (S)-1,2-propanediol; TGA weight loss corresponds to 0.48 equivalents of (S)-1,2-propanediol) |

Form I exhibited minimal weight loss (~0.51%) upon heating to 150 °C in TGA, and only a minor acetone signal was detected at 2.09 ppm in $^1$H NMR spectrum, with integration indicating approximately 0.06 equivalents. In the DSC curve, a sharp endothermic peak was observed at 209.2 °C (peak temperature). Baseline perturbation occurred prior to this event, accompanied by concurrent mass loss in TGA, indicating that melting and decomposition occur simultaneously. These observations support its assignment as an anhydrous form.

Forms II, III, and K1 showed no detectable organic solvent signals in the $^1$H NMR spectra. In TGA, all three exhibited distinct stepwise weight-loss events, with corresponding thermal signals observed in DSC, consistent with typical hydrate behavior. Moreover, the relatively low dehydration temperatures suggest that the observed weight-loss steps in TGA are minimally affected by high-temperature degradation. The stepwise TGA weight-losses observed for Forms II and III are in good agreement with the theoretical values for a trihydrate and a dihydrate, respectively, supporting their assignments. The assignments of Forms I–III are consistent with those reported in the patent. However, Form K1 exhibits a TGA weight loss of 15.7%, corresponding to approximately 4.8 equivalents of water, which does not by itself support a definitive stoichiometric assignment.

The assignment of solvated forms appears considerably more complex. For some solvates, the results from different techniques are self-consistent. Although the solvent stoichiometry estimated

from TGA and $^{1}$H NMR may show minor deviations, they are generally close to integer ratios, allowing for preliminary identification. For example, Type A exhibited a weight-loss step up to 170 °C in TGA, with a corresponding thermal event at 140 °C in DSC. $^{1}$H NMR (integration of the signals at 1.38-1.13 ppm) agreed with the TGA weight loss, both indicating approximately one equivalent of solvent per API molecule. Therefore, Type A was identified as a mono-ethyl lactate solvate.

When multiple techniques indicate a non-integer stoichiometry, assignment becomes significantly more challenging. Form CS14 showed a weight-loss step up to 160 °C and a melting event at 148.8 °C (peak temp) in DSC. $^{1}$H NMR integration indicated approximately 1.0 equivalent of acetylacetone, while TGA result suggested 0.87 equivalents. Similarly, Form K3 exhibited 0.36 equivalents of acetonitrile by $^{1}$H NMR. A two-step weight loss was observed in TGA, corresponding to two distinct thermal events in DSC at 79.0 °C and 128.5 °C. The total TGA weight loss corresponds to 0.56 equivalents of acetonitrile, with contributions of 0.23 and 0.33 equivalents for the two steps. In these cases, the solvent signals of acetonitrile and acetylacetone in the $^{1}$H NMR spectra partially overlap with those of the API, introducing additional uncertainty in form identification.

For other solvated forms, pronounced inconsistencies between techniques preclude reliable assignment. For Type D, $^{1}$H NMR integration (based on the signal at 4.71-4.25 ppm) indicated approximately 1.01 equivalent of glycerol, whereas TGA weight loss between 110–165 °C corresponded to only 0.24 equivalents. For Type F, $^{1}$H NMR (based on the signal at 1.00 ppm) suggested approximately 0.88 equivalent of 1,2-propanediol, while TGA mass loss between 110–160 °C corresponded to only 0.48 equivalents.

Additionally, a notable case was encountered during the characterization of Type H. In TGA, Type H exhibited a two-step weight-loss profile. It was prepared in a DCM/acetonitrile system. However, $^{1}$H NMR analysis revealed no detectable signals corresponding to either acetonitrile or DCM. Subsequent XRPD analysis of the small portion used for NMR test confirmed a solid-form

conversion, yielding a new hydrate designated Form CS13. XRPD of the freshly dried material was consistent with Type H, whereas material stored at room temperature showed partial conversion to Form CS13 and contained a mixture of the two forms. This conversion complicated the assignment of Type H by conventional solid-state characterization.

Collectively, these results highlight the limitations of conventional solid-state characterization. Even when results from multiple techniques are consistent, these methods cannot directly confirm molecular packing or guest content, nor establish whether an apparent hydrate contains water in the crystal lattice or merely retains surface water. For solvated forms, inconsistent solvent stoichiometries derived from TGA and $^{1}$H NMR can further complicate assignment. These limitations are particularly consequential for crystalline powders that do not yield crystals suitable for SC-XRD. ED directly addresses this gap by providing crystal structures from such materials. Supporting XRPD, TGA, DSC, and $^{1}$H NMR data are provided in Supplementary Figs. 14–54.

### 3.3 Electron diffraction structure determination

For eight of the ten selected solid forms, three distinct sample preparation methods were submitted for ED experiments: vacuum-dried solids, room-temperature air-dried solids (prepared by separating a portion of the suspension using a filter centrifuge tube; after centrifugation, the centrifuged solid collected in the inner tube was exposed to ambient room conditions to obtain a near-dry sample), and samples preserved in their mother liquor. For Form K1 (provisional tetrahydrate assignment), only the room-temperature air-dried solid and the suspension were provided. Only vacuum-dried material was submitted directly as Type H (mono-ACN solvate). An additional Type H structure was subsequently obtained from a mother-liquor vial originally submitted as Form K3 (hemi-ACN solvate) after the Form K3 suspension underwent conversion to Type H.

The available preparations were compared to assess how sample presentation and grid preparation and transfer affected diffraction-data quality, structure determination, and solid-form preservation. Because not every solid form was evaluated under every combination of sample presentation and grid-preparation method, the study was not a complete factorial comparison; the resulting comparisons are therefore descriptive rather than estimates of the independent effect of each variable.

Three experimental factors should be distinguished: sample presentation (vacuum-dried solid, room-temperature air-dried solid, or mother-liquor suspension), grid preparation and transfer (room-temperature or cryogenic), and measurement temperature. In this study, 'cryogenic preparation' denotes placing the sample on the TEM grid and blotting, where applicable, at room temperature, followed by plunge cooling of the loaded grid, and cryogenic transfer. It does not denote applying the sample directly to a cryogenically cooled grid. 'Room-temperature preparation' in Table 3 denotes grid loading and transfer without plunge cooling, i.e. room-temperature transfer; these grids were cooled inside the diffractometer before measurement. All final datasets reported here and deposited with the CCDC were collected at 123(2) K. For vacuum-dried or room-temperature air-dried samples, a small quantity of solid was placed directly on the TEM grid. For mother-liquor suspensions, a drop was placed on the grid and excess liquid was blotted at room temperature. Under the cryogenic preparation, the loaded grid and holder were then plunged into liquid nitrogen and transferred through the pre-chamber of the electron diffractometer under cryogenic conditions.

Vacuum-dried samples subjected to room-temperature grid preparation and transfer generally produced lower-quality ED data for the hydrate and solvate forms evaluated. Observed limitations included low resolution, smeared diffraction spots, and, in several cases, insufficient data for structure solution. These observations are consistent with loss of long-range order following removal of guest water or solvent from forms whose packing depends on those

molecules. The sharpness of XRPD peaks from the dried samples did not necessarily predict the deterioration later evident in the ED data.

Room-temperature air-dried samples also gave variable results. For several forms, partial loss of water or solvent during room-temperature transfer and vacuum exposure before cooling was associated with reduced crystallinity or incompletely defined water or solvent content in the resulting structural models. Cryogenic preparation improved the outcome for some room-temperature air-dried samples, although the guest-molecule occupancies were not always as completely defined as in the corresponding mother-liquor preparations.

Across the preparation combinations evaluated, mother-liquor suspensions combined with the cryogenic preparation produced the most consistently complete refinements for the labile hydrates and solvates. This combined approach improved the results for several forms and enabled satisfactory structure determination of multiple solid forms, including Type D (mono-glycerol solvate) and Type F ((S)-1,2-propanediol solvate), for which the corresponding dried preparations did not provide accurate results. However, mother-liquor preservation was not required for every form: Form I (anhydrate) and Type H (mono-ACN solvate) were solved from vacuum-dried samples, and Form K3 (hemi-ACN solvate) was solved and refined from a room-temperature air-dried sample.

The dedicated electron diffractometer used here includes a sample holder, transfer unit, and pre-chamber that support the cryogenic preparation for solid or for liquid-suspended samples. Rapid cryogenic plunging before transfer can help preserve labile crystalline forms during handling and exposure to high vacuum. The present study supports this approach particularly for hydrates and solvates that are susceptible to guest loss, while also showing that satisfactory results can be obtained from dried preparations for some more stable forms.

Because mother-liquor preservation and the cryogenic preparation were often applied together, and because not all forms were evaluated under every preparation combination, their independent contributions cannot be quantified from this dataset. The appropriate practical conclusion is

therefore that ED sample handling should be matched to solid-form stability, with mother-liquor preservation combined with the cryogenic preparation prioritized for labile hydrates and solvates rather than treated as a universal default.

Among the vacuum-dried samples evaluated using room-temperature grid preparation and transferred at room temperature, Form I (anhydrate), Type H (mono-ACN solvate), and Type A (ethyl L-lactate solvate) yielded diffraction data sufficient for structure determination. For Type A, however, prior knowledge of the solvate identity was needed to model the guest molecule satisfactorily with constraints and restraints. Form IV (anhydrate), which was not one of the ten selected forms, was also identified in the vacuum-dried sample from Form II. Its structure was determined and deposited with the CCDC.

Room-temperature air-dried Form II (trihydrate) and Form III (dihydrate) samples subjected to the cryogenic preparation yielded structures in which the hydrate identities were established, although the water sites refined with partial occupancy. In contrast, Form K3 (hemi-ACN solvate) was solved and refined from a room-temperature air-dried sample using room-temperature grid preparation and transfer, with unambiguous refinement of the acetonitrile solvate. Mother-liquor preparations of these two forms (Form II and Form III) provided additional confirmation of the guest content and a 100% occupancy for the water molecules in the crystal lattice.

Type D (mono-glycerol solvate) and Type F (1,2-propanediol solvate) were solved and refined satisfactorily only from mother-liquor suspensions subjected to the cryogenic preparation.

Vacuum-dried Form CS14 (acetylacetone solvate) produced a structure solution from lower-quality data, whereas the mother-liquor suspension subjected to cryogenic preparation delivered a satisfactory solution and refinement.

As mentioned before, Type A (ethyl L-lactate solvate) yielded a structure from the vacuum-dried powder using room-temperature grid preparation, although prior knowledge of the solvate identity was needed to model the guest molecule. A subsequent measurement of a mother-liquor

suspension processed using cryogenic preparation produced higher-quality data, allowing the solvate molecule to be identified, modeled, and refined without constraints.

The original Type H (mono-ACN solvate) submission consisted only of vacuum-dried material and yielded the expected mono-acetonitrile solvate structure. Type H was also identified in a mother-liquor vial originally submitted as Form K3 (hemi-ACN solvate), demonstrating that the Form K3 suspension had undergone conversion to Type H. Processing this suspension using the cryogenic preparation produced higher-quality diffraction data than the original dried Type H sample, enabling more complete refinement of the acetonitrile solvate. The Type H structure reported here and deposited with the CCDC was refined from this higher-quality dataset.

Table 3 summarizes the results obtained using the different sample presentations and grid-preparation methods. All reported structures and CCDC-deposited datasets were measured at low temperature.

**Table 3 | ED results for the different sample presentations and grid-preparation methods.**

| Intended Form | Sample form | Sample prep. | Result | Comments |
|---|---|---|---|---|
| **Form I** | vacuum-dried solids | Room-temperature preparation | Structure solved and refined | |
| **Form II** | vacuum-dried solids | Room-temperature preparation | No Form II structure obtained | The structure obtained was Form IV (anhydrate) and it is deposited with the CCDC. |
| | room-temperature air-dried solids | Cryogenic preparation | Structure solved and refined | Hydration state unambiguous; three water sites refined with partial occupancy. |
| | mother-liquor suspension | Cryogenic preparation | Structure solved and refined | Three water sites refined at 100% occupancy. |
| **Form III** | room-temperature air-dried solids | Cryogenic preparation | Structure solved and refined | Hydration state unambiguous; two water sites refined with partial occupancy. |
| | mother-liquor suspension | Cryogenic preparation | Structure solved and refined | Two water sites refined at 100% occupancy. |
| **Form CS14** | vacuum-dried solids | Cryogenic preparation | Structure solved | Crystal quality was insufficient for full refinement. |

| Intended Form | Sample form | Sample prep. | Result | Comments |
|---|---|---|---|---|
| | mother-liquor suspension | Cryogenic preparation | Structure solved and refined | Structure solved and refined satisfactorily. |
| **Type A** | vacuum-dried solids | Room-temperature preparation | Structure solved and refined | Modeling the solvate required extensive restraints and constraints and prior knowledge of its identity. |
| | mother-liquor suspension | Cryogenic preparation | Structure solved and refined | Data quality was substantially improved, allowing refinement of the solvate molecule without restraints. |
| **Type D** | mother-liquor suspension | Cryogenic preparation | Structure solved and refined | Good-quality structure; solvate fully identified. |
| **Type F** | mother-liquor suspension | Cryogenic preparation | Structure solved and refined | Good-quality structure; solvate fully identified. |
| **Type H** | vacuum-dried solids | Room-temperature preparation | Structure solved and refined | Good-quality structure; solvate fully identified. |
| | Form K3 mother-liquor suspension; underwent conversion to Type H | Cryogenic preparation | Structure solved and refined | Higher-quality Type H dataset used for the reported structure and CCDC deposition. |
| **Form K1** | room-temperature air-dried solids | Cryogenic preparation | Structure solved and refined; identified as Form II | ED analysis of the room-temperature air-dried submission yielded Form II, whereas XRPD of the remaining air-dried material retained the Form K1 pattern. This suggests that the aliquot analyzed by ED converted to Form II (trihydrate) during grid preparation, transfer, and/or measurement. |
| | mother-liquor suspension | Cryogenic preparation | Structure solved and refined; identified as Form II | ED analysis after shipment and several weeks of storage yielded Form II. XRPD showed Form K1 in the freshly prepared suspension but complete conversion to Form II after ambient storage, indicating that conversion occurred before ED sample preparation and analysis. |
| **Form K3** | room-temperature air-dried solids | Room-temperature preparation | Structure solved and refined | Unambiguous refinement of the solvate molecule. |
| | mother-liquor suspension | Cryogenic preparation | Structure solved and refined | Acetonitrile fully identified; hemi-acetonitrile solvate confirmed. |

Table 3 shows that successful structures were obtained through more than one preparation pathway. Mother-liquor suspension combined with the cryogenic preparation was particularly valuable for labile hydrates and solvates. A higher-quality Type H (mono-ACN solvate) dataset was subsequently obtained from a mother-liquor vial originally submitted as Form K3 after the suspension underwent conversion to Type H.

If only vacuum-dried and room-temperature air-dried samples had been evaluated, structure determination or complete guest-molecule refinement would have been compromised for several of the labile forms in this set. The mother-liquor suspensions processed using the cryogenic preparation provided better-defined structures in those cases. These findings identify sample presentation and grid preparation as important, stability-dependent variables in ED experiments, but they do not support a single universal preparation protocol. All structures determined by ED have been deposited with the Cambridge Crystallographic Data Centre (CCDC), and the corresponding crystallographic ED data are summarized in Table 4.

Form II (trihydrate) illustrates the influence of sample handling on form identity. ED analysis of the vacuum-dried sample yielded an anhydrous structure whose simulated XRPD pattern differed markedly from the experimental XRPD pattern of Form II and instead agreed with Form IV, a known anhydrous form not included among the ten selected forms. A subsequent measurement of a mother-liquor suspension processed using the cryogenic preparation yielded the Form II trihydrate structure, supported by agreement between the simulated and experimental XRPD patterns. This comparison is consistent with loss of water during drying or subsequent handling and shows that an ED structure obtained from a dried specimen may not represent the solid form characterized before drying. For labile hydrates such as Form II, solid-form-preserving preparation and cross-validation against conventional solid-state data are therefore important.

The case of Type H (mono-ACN solvate) provides a further instructive example. The initial ED measurement on the dried sample unambiguously yielded the crystal structure of the expected acetonitrile (ACN) solvate. However, a repeat measurement on the same dried sample approximately two to three months later revealed measurable deterioration in crystallinity: diffraction data quality had declined, and although the structure could still be solved and refined satisfactorily, the crystallographic occupancy of the ACN molecule had decreased relative to the original measurement. This indicates that Type H (mono-ACN solvate) is stable under ambient conditions for a limited period, after which solvent molecules progressively vacate the crystal lattice. Such desolvation leads to a gradual deterioration in long-range crystalline order, as directly observed in the ED experiments. The associated consequences are significant: partial loss of the solvate molecule over time would be expected to produce changes in the XRPD pattern, potentially leading to misinterpretation of the form's identity, stability, or persistence under storage conditions.

**Table 4 | Crystallographic ED data for all structures determined.**

| Solid Form Name | Form I | Form II | Form III | Form IV† | Form K3 |
|---|---|---|---|---|---|
| **Empirical formula** | $C_{26}H_{23}N_7O_2$ | $C_{26}H_{29}N_7O_5$ | $C_{26}H_{27}N_7O_4$ | $C_{26}H_{23}N_7O_2$ | $C_{27}H_{24.5}N_{7.5}O_2$ |
| **Formula weight** | 465.51 | 519.56 | 501.55 | 465.51 | 486.04 |
| **Temperature / K** | 123.15 | 123(2) | 123(2) | 123(2) | 123.15 |
| **Crystal system** | triclinic | orthorhombic | monoclinic | orthorhombic | orthorhombic |
| **Space group** | *P1* | $P2_12_12$ | $P2_1$ | $P2_12_12$ | $P2_12_12_1$ |
| **a, b, c / Å** | 8.0876(10)<br>10.3108(10)<br>14.2960(19) | 18.9734(6)<br>26.7615(17)<br>5.0340(2) | 8.2787(9)<br>21.160(2)<br>14.1233(17) | 18.1470(7)<br>25.4262(19)<br>4.9980(2) | 13.8503(9)<br>15.9114(10)<br>22.624(2) |
| **α, β, γ / °** | 85.892(11)<br>75.650(10)<br>82.167(10) | 90 | 90<br>94.434(11)<br>90 | 90 | 90 |
| **Volume / Å³** | 1143.3(2) | 2556.0(2) | 2466.7(5) | 2306.1(2) | 4985.8(7) |
| **Z** | 2 | 4 | 4 | 4 | 8 |
| **ρcalc / g cm⁻³** | 1.352 | 1.350 | 1.351 | 1.341 | 1.295 |
| **F(000)** | 194.0 | 424.0 | 412.0 | 387 | 810.0 |
| **Crystal colour** | colourless | colourless | colourless | colourless | colourless |

| Solid Form Name | Form I | Form II | Form III | Form IV† | Form K3 |
|---|---|---|---|---|---|
| **Radiation (electron)** | λ = 0.02851 Å | λ = 0.02851 Å | λ = 0.02851 Å | λ = 0.02851 Å | λ = 0.02851 Å |
| **Data sets used (merged)** | 7 | 6 | 9 | 14 | 13 |
| **Resolution (Å) / completeness** | 0.90 / 99.7% | 0.90 / 99.8% | 0.90 / 99.9% | 0.90 / 99.9% | 0.90 / 100% |
| **2θ range for data collection / °** | 0.16 to 1.814 | 0.106 to 1.814 | 0.154 to 1.814 | 0.13 to 1.82 | 0.126 to 1.814 |
| **Index ranges** | −8 ≤ h ≤ 8<br>−11 ≤ k ≤ 11<br>−15 ≤ l ≤ 15 | −21 ≤ h ≤ 21<br>−29 ≤ k ≤ 28<br>−5 ≤ l ≤ 5 | −9 ≤ h ≤ 9<br>−23 ≤ k ≤ 23<br>−15 ≤ l ≤ 15 | −20 ≤ h ≤ 20<br>−28 ≤ k ≤ 28<br>−5 ≤ l ≤ 5 | −15 ≤ h ≤ 15<br>−17 ≤ k ≤ 17<br>−25 ≤ l ≤ 25 |
| **Reflections collected** | 20782 | 51399 | 47132 | 99938 | 163051 |
| **Independent reflections** | 6494<br>$R_{int}$ = 0.5477<br>$R_{sigma}$ = 0.3805 | 3681<br>$R_{int}$ = 0.2141<br>$R_{sigma}$ = 0.1217 | 7090<br>$R_{int}$ = 0.3661<br>$R_{sigma}$ = 0.2460 | 3319<br>$R_{int}$ = 0.7138<br>$R_{sigma}$ = 0.1717 | 7186<br>$R_{int}$ = 0.9167<br>$R_{sigma}$ = 0.2356 |
| **Data/restraints/parameters** | 6494/873/634 | 3681/540/363 | 7090/908/622 | 3319/601/320 | 7186/1059/660 |
| **Goodness-of-fit on $F^2$** | 1.000 | 1.198 | 1.030 | 1.187 | 1.167 |
| **Final R indexes [I ≥2σ (I)]** | $R_1$ = 0.1115,<br>w$R_2$ = 0.2566 | $R_1$ = 0.1249,<br>w$R_2$ = 0.3009 | $R_1$ = 0.1570,<br>w$R_2$ = 0.3680 | $R_1$ = 0.1482<br>w$R_2$ = 0.3167 | $R_1$ = 0.1592,<br>w$R_2$ = 0.3492 |
| **Final R indexes [all data]** | $R_1$ = 0.1576,<br>w$R_2$ = 0.2768 | $R_1$ = 0.1408,<br>w$R_2$ = 0.3057 | $R_1$ = 0.2228,<br>w$R_2$ = 0.4064 | $R_1$ = 0.1690<br>w$R_2$ = 0.3229 | $R_1$ = 0.1897,<br>w$R_2$ = 0.3698 |
| **Largest diff. peak/hole / e $Å^{-3}$** | 0.15/−0.18 | 0.15/−0.16 | 0.22/−0.17 | 0.18/−0.18 | 0.34/−0.24 |
| **CCDC number** | 2548852 | 2548853 | 2554539 | 2554541 | 2548854 |

† Form IV was not submitted as a separate sample; it was identified in the vacuum-dried Form II submission. Its crystallographic data and CCDC deposition number are included here.

| Solid Form Name | Form CS14 | Type A | Type H | Type D | Type F |
|---|---|---|---|---|---|
| **Empirical formula** | $C_{31}H_{31}N_7O_4$ | $C_{31}H_{33}N_7O_5$ | $C_{28}H_{26}N_8O_2$ | $C_{29}H_{31}N_7O_5$ | $C_{29}H_{31}N_7O_4$ |
| **Formula weight** | 565.63 | 583.64 | 506.57 | 557.61 | 541.61 |
| **Temperature / K** | 123.15 | 123.15 | 123(2) | 123(2) | 123.15 |
| **Crystal system** | orthorhombic | triclinic | orthorhombic | orthorhombic | orthorhombic |
| **Space group** | $P2_12_12_1$ | $P1$ | $P2_12_12$ | $P2_12_12$ | $P2_12_12_1$ |
| **a, b, c / Å** | 4.98061(8)<br>16.8733(6)<br>33.2528(6) | 7.4740(3)<br>13.0497(4)<br>15.3056(14) | 16.5320(14)<br>27.534(11)<br>5.3733(9) | 19.504(4)<br>26.353(5)<br>5.2917(11) | 5.5084(5)<br>14.6023(14)<br>33.488(5) |
| **α, β, γ / °** | 90 | 85.194(4)<br>85.025(5)<br>83.869(3) | 90 | 90 | 90 |
| **Volume / $Å^3$** | 2794.55(12) | 1474.49(15) | 2445.9(10) | 2719.9(9) | 2693.6(5) |
| **Z** | 4 | 2 | 4 | 4 | 4 |
| **ρcalc / g $cm^{-3}$** | 1.344 | 1.315 | 1.376 | 1.362 | 1.336 |
| **F(000)** | 470.0 | 241.0 | 423.0 | 458.0 | 450.0 |
| **Crystal colour** | colourless | colourless | colourless | colourless | colourless |
| **Radiation (electron)** | λ = 0.02851 Å | λ = 0.02851 Å | λ = 0.02851 Å | λ = 0.02851 Å | λ = 0.02851 Å |

| Solid Form Name | Form CS14 | Type A | Type H | Type D | Type F |
|---|---|---|---|---|---|
| **Data sets used (merged)** | 8 | 16 | 10 | 12 | 9 |
| **Resolution (Å) / completeness** | 0.90 / 100% | 0.90 / 96.6% | 0.99 / 84.6%‡ | 1.00 / 96.8% | 0.90 / 98.6% |
| **2θ range for data collection / °** | 0.098 to 1.814 | 0.126 to 1.814 | 0.266 to 1.642 | 0.104 to 1.634 | 0.268 to 1.816 |
| **Index ranges** | $-5 \le h \le 5$<br>$-18 \le k \le 18$<br>$-36 \le l \le 36$ | $-8 \le h \le 8$<br>$-14 \le k \le 14$<br>$-16 \le l \le 16$ | $-16 \le h \le 16$<br>$-25 \le k \le 25$<br>$-5 \le l \le 5$ | $-19 \le h \le 19$<br>$-25 \le k \le 26$<br>$-5 \le l \le 5$ | $-6 \le h \le 6$<br>$-16 \le k \le 16$<br>$-36 \le l \le 36$ |
| **Reflections collected** | 84210 | 74437 | 12709 | 101131 | 29647 |
| **Independent reflections** | 4028<br>$R_{int}$ = 0.4129<br>$R_{sigma}$ = 0.1340 | 8121<br>$R_{int}$ = 0.5077<br>$R_{sigma}$ = 0.5515 | 2292<br>$R_{int}$ = 0.2088,<br>$R_{sigma}$ = 0.1389 | 2792<br>$R_{int}$ = 0.4405<br>$R_{sigma}$ = 0.1723 | 3843<br>$R_{int}$ = 0.3114<br>$R_{sigma}$ = 0.2704 |
| **Data/restraints/parameters** | 4028/627/380 | 8121/1219/790 | 2292/546/345 | 2792/778/414 | 3843/566/370 |
| **Goodness-of-fit on $F^2$** | 1.265 | 1.076 | 1.511 | 1.184 | 1.125 |
| **Final R indexes [I≥2σ (I)]** | $R_1$ = 0.1379,<br>$wR_2$ = 0.3306 | $R_1$ = 0.1287,<br>$wR_2$ = 0.2949 | $R_1$ = 0.1577,<br>$wR_2$ = 0.3674 | $R_1$ = 0.1937,<br>$wR_2$ = 0.4464 | $R_1$ = 0.1727,<br>$wR_2$ = 0.3537 |
| **Final R indexes [all data]** | $R_1$ = 0.1480,<br>$wR_2$ = 0.3371 | $R_1$ = 0.1820,<br>$wR_2$ = 0.3145 | $R_1$ = 0.1680,<br>$wR_2$ = 0.3734 | $R_1$ = 0.2113,<br>$wR_2$ = 0.4515 | $R_1$ = 0.1898,<br>$wR_2$ = 0.3728 |
| **Largest diff. peak/hole / e $Å^{-3}$** | 0.27/-0.22 | 0.23/−0.21 | 0.19/-0.20 | 0.20/−0.18 | 0.21/-0.17 |
| **CCDC number** | 2548858 | 2548855 | 2548857 | 2554544 | 2548856 |

‡The completeness of this dataset (84.6%) is lower than that of the other datasets, mainly due to the low diffraction quality and weak intensities at higher angles observed for the Type H sample. Nevertheless, a completeness of 84.6% is still considered reasonable for ED data.[25]

## 3.4 Comparison with conventional characterization

**Table 5 | ED structure-determination results and comparison with conventional solid-state characterization.**

| Solid Form | Preliminary Identification based on TGA and $^1$H NMR | Identification based on ED result |
|---|---|---|
| **Form I** | **Anhydrate** | **Anhydrate** |
| **Form II** | **Trihydrate**<br>(theoretical water content of a trihydrate is 10.4%) | **Form IV** (first measurement on dried sample)<br>**Trihydrate** (second measurement, mother-liquor suspension) |
| **Form III** | **Dihydrate**<br>(theoretical water content of a dihydrate is 7.2%) | **Dihydrate** |

| Solid Form | Preliminary Identification based on TGA and $^1$H NMR | Identification based on ED result |
|---|---|---|
| **Form K1** | **Provisional tetrahydrate assignment** (TGA: approximately 4.8 equivalents of water; DVS: approximately 4.1 equivalents of water at 20% RH) | **Trihydrate (Form II)**, room-temperature air-dried submission<br>**Trihydrate (Form II)**, mother-liquor suspension<br>The air-dried ED aliquot likely converted during grid preparation, transfer, or measurement, whereas the mother-liquor suspension converted during shipment or storage before ED analysis. |
| **Form K3** | **Acetonitrile solvate** ($^1$H NMR signal corresponds to 0.36 equivalents of acetonitrile; TGA weight loss corresponds to ~0.23 and ~0.33 equivalents of acetonitrile for the two steps) | **Hemi-acetonitrile solvate** |
| **Form CS14** | **Acetylacetone solvate** ($^1$H NMR signal corresponds to 1.0 equivalents of acetylacetone; TGA weight loss corresponds to 0.87 equivalents of acetylacetone) | **Mono-acetylacetone solvate** |
| **Type A** | **Mono-ethyl L-lactate solvate** ($^1$H NMR signal corresponds to 0.95 equivalents of ethyl L-lactate; TGA weight loss corresponds to 0.97 equivalents of ethyl L-lactate) | **Mono-ethyl L-lactate solvate** |
| **Type H** | **Uncertain** (TGA weight loss corresponds to ~0.52 and ~0.33 equivalents of acetonitrile for the two steps. A solid-form conversion occurred during storage) | **Mono-acetonitrile solvate** |
| **Type D** | **Glycerol solvate** ($^1$H NMR signal corresponds to 1.01 equivalents of glycerol; TGA weight loss corresponds to 0.24 equivalents of glycerol) | **Mono-glycerol solvate** |
| **Type F** | **(S)-1,2-Propanediol solvate** ($^1$H NMR signal corresponds to 0.88 equivalents of (S)-1,2-propanediol; TGA weight loss corresponds to 0.48 equivalents of (S)-1,2-propanediol**)** | **Mono-(S)-1,2-propanediol solvate** |

Table 5 compares the ED structure-determination results with the preliminary solid-form identification results obtained by conventional solid-state characterization. For the anhydrous Form I and Form IV, the hydrate Form III, and all six solvated forms, the simulated XRPD patterns generated from the ED-derived structures show excellent agreement with the experimental powder XRPD data, validating the reliability of ED for structure determination

across diverse solid forms. For solvates exhibiting non-integer stoichiometry in conventional solid-state characterization, ED provides definitive structural assignments that are otherwise challenging. Supporting XRPD comparisons and DVS data are provided in Supplementary Figs. 1–13.

This advantage is particularly evident for Type D (mono-glycerol solvate) and Type F ((S)-1,2-propanediol solvate), where significant discrepancies were observed between $^{1}$H NMR and TGA results. In both cases, the ED-derived structures are consistent with the NMR data. To investigate the relatively small mass-loss steps observed in TGA, additional heating experiments were performed. After being heated to the corresponding TGA transition temperature (e.g., 144 °C for Type D) and then cooled to room temperature, the samples showed extensive chemical degradation, with HPLC purity decreasing to 4.12%. This finding indicates that decomposition contributed substantially to the observed mass loss. Because degradation and solvent release may overlap, their relative contributions cannot be quantified from the TGA data alone.

ED, combined with XRPD, can characterize individual components within solid-form mixtures. The freshly dried Type H material was consistent with Type H but partially converted to Form CS13 during ambient storage. ED determined Type H to be a mono-acetonitrile solvate. Comparison of its simulated XRPD pattern with the experimental patterns of the freshly dried and ambient-stored materials showed that the additional reflections in the stored sample were attributable to Form CS13, confirming the coexistence of Type H and Form CS13. This illustrates how crystallite-specific ED can determine the structure of one component, while comparison with bulk XRPD can reveal and identify additional solid forms. This combined approach is particularly valuable when individual forms are difficult to isolate from mixtures.

The results also show that ED can reveal solid-form conversion associated with sample preparation or measurement conditions. For Form II (trihydrate), the structure determined from the dried sample did not match the experimental XRPD pattern of Form II but instead showed excellent agreement with Form IV (anhydrate), an anhydrous form identified independently by

VT-XRPD. DVS measurements showed that Form II dehydrates below 10% relative humidity, consistent with conversion during drying, transfer, or exposure to vacuum. When a mother-liquor suspension was subsequently used for ED analysis, the Form II (trihydrate) structure was obtained, and its simulated XRPD pattern showed excellent agreement with the experimental powder diffraction pattern of Form II. These observations support dehydration-associated conversion from Form II to Form IV, although the conversion pathway was not directly observed. ED datasets from both the room-temperature air-dried and mother-liquor submissions yielded Form II (trihydrate) rather than Form K1 (provisional tetrahydrate assignment). TGA indicated that the originally isolated Form K1 contained more water than Form II. XRPD of the remaining air-dried material retained the Form K1 pattern, suggesting that the ED aliquot converted during grid preparation, transfer, or measurement. By contrast, XRPD showed Form K1 in the freshly prepared mother-liquor suspension but complete conversion to Form II after shipment and several weeks of ambient storage, indicating that the suspension had converted before ED sample preparation and analysis. The two submissions therefore had different conversion histories.

The hydration state of Form K1 was further investigated using dynamic vapor sorption (DVS) analysis on the room-temperature air-dried sample. The DVS profile exhibited a distinct inflection point during the desorption process. Moisture loss proceeded relatively slowly between 95% RH and 20% RH, which is attributed to surface-adsorbed water, whereas rapid desorption of crystalline water occurred below 20% RH. Upon completion of the full DVS cycle, the sample exhibited a significant loss of crystallinity and became nearly amorphous. These results further indicate that Form K1 possesses a highly labile hydration state and is prone to structural collapse upon dehydration. Based on the water content at 20% RH, Form K1 is estimated to contain approximately 4.1 equivalents of water. On the basis of the combined TGA and DVS results, Form K1 is provisionally assigned as a tetrahydrate; however, this assignment was not confirmed by direct crystal-structure determination.

Form K1 is therefore the only form among the ten for which the originally selected solid form could not be structurally confirmed. Accordingly, ED successfully determined crystal structures from all ten submitted samples (Fig. 1), while confirming the originally selected solid form in nine cases. Form K1, provisionally assigned as a tetrahydrate, yielded Form II rather than the originally selected solid form.

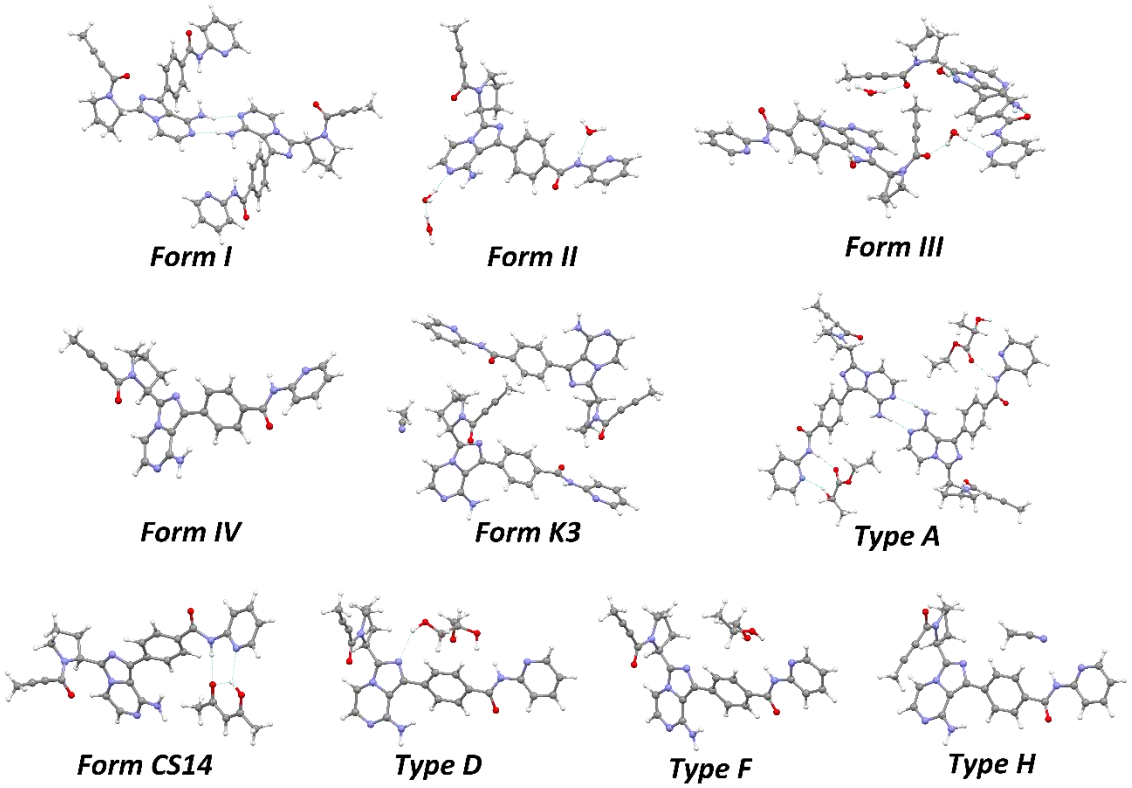



**Fig. 1 |** Crystal structures determined by ED in this study. Form IV was identified incidentally from the Form II vacuum-dried sample and is also included. Form K1, provisionally assigned as a tetrahydrate based on TGA and DVS, yielded Form II from both submissions. The mother-liquor suspension converted before ED preparation, whereas the air-dried ED aliquot likely converted during grid preparation, transfer, or measurement.

### 3.5 Structural basis of extensive polymorphism revealed by comparison of ED-determined crystal forms

By resolving multiple crystal structures of acalabrutinib, spanning a broad range of solvation and hydration states, it becomes possible to directly compare structural similarities and differences across its solid-form landscape within a unified framework. In addition to validating ED as a robust structure-determination technique, these data provide key mechanistic insight into the molecular origins of acalabrutinib's pronounced solid-form diversity. Overall, the observed structural landscape arises from the concerted interplay of molecular conformational flexibility, diverse hydrogen-bonding possibilities, and the ability of the crystal lattice to accommodate a wide range of guest molecules.

At the molecular level, acalabrutinib contains four major rotatable bonds (τ1–τ4, Fig. 2), enabling multiple torsional states and thereby accessing a range of low-energy conformations in the solid state. The availability of these conformations provides a structural basis for diverse intermolecular interaction modes and packing arrangements. Comparative analysis of the resolved crystal structures reveals pronounced variations in key torsion angles across different forms (Table 6), reflecting a high degree of conformational adaptability. In particular, torsional degrees of freedom associated with hydrogen-bond donor and acceptor orientations (τ1, τ3, and τ4) further expand the range of accessible hydrogen-bonding networks.

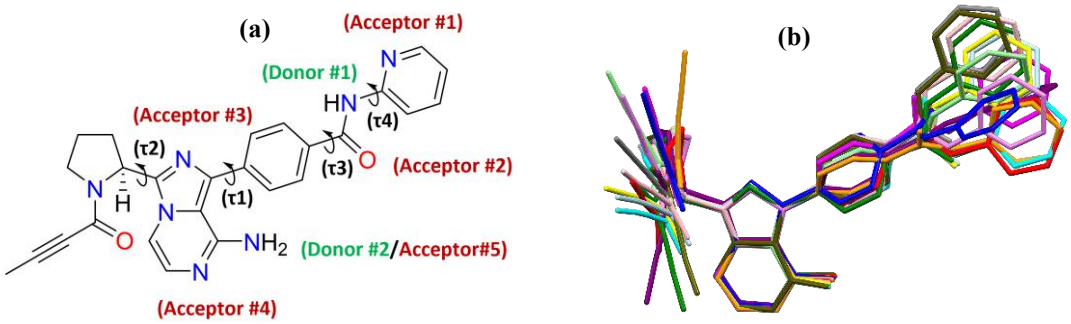



**Fig. 2** | Chemical structure of acalabrutinib and conformational comparison of the acalabrutinib molecule found in ten solid forms. (a). Chemical structure marking the major torsion angles and hydrogen bond donors and acceptors. (b). Conformational overlay of API molecules in different polymorphs. For clarity, all hydrogen atoms and solvate / hydrate molecules have been omitted.

**Table 6 | Key torsion angles of the acalabrutinib molecule in the different solid forms.**

| Solid form (Z') | Crystallographically independent molecules | Torsion angle τ1 | Torsion angle τ2 | Torsion angle τ3 | Torsion angle τ4 |
|---|---|---|---|---|---|
| **Form I (Z'=2)** | 1st molecule | 54.9(19)° | -67.8(16)° | 13(2)° | 41(2)° |
| | 2nd molecule | 53(2)° | -19.1(19)° | 1(2)° | -35(3)° |
| **Form IV (Z'=1)** | N.A | 33(2)° | -64(2)° | -25(3)° | -31(3)° |
| **Form II (Z'=1)** | N.A | 32(2)° | -65.2(18)° | -34(2)° | -18(3)° |
| **Form III (Z'=2)** | 1st molecule | 40(2)° | -22(3)° | -6(3)° | -2(3)° |
| | 2nd molecule | -43(2)° | -57(3)° | 17.6(11)° | 19(3)° |
| **Form K3 (Z'=2)** | 1st molecule | -46(2)° | -32(3)° | -27(2)° | 13(3)° |
| | 2nd molecule | 56.8(19)° | -48(2)° | 33(3)° | -6(3)° |
| **Type H (Z'=1)** | N.A | 20(3)° | -53(3)° | -26(3)° | 14(4)° |
| **Form CS14 (Z'=1)** | N.A | 25.5(18)° | -67.5(17)° | -24.6(19)° | -32(2)° |
| **Type A (Z'=2)** | 1st molecule | -31.7(17)° | -35.2(18)° | 12.6(19)° | 39(2)° |
| | 2nd molecule | 38.5(15)° | -38.6(15)° | -10(2)° | -20.2(19)° |
| **Type D (Z'=1)** | N.A | 39 (4)° | -69(3)° | -30(2)° | 18(4)° |
| **Type F (Z'=1)** | N.A | 28.6(17)° | -53.8(17)° | -27(2)° | 9(2)° |

As a representative example, Form K3 (hemi-ACN solvate) comprises two crystallographically independent API molecules together with one acetonitrile (ACN) solvate per asymmetric unit, corresponding to a hemi-ACN solvate (Z′ = 2). Structural superposition of the two independent

API conformers reveals that they adopt markedly distinct molecular geometries within the same crystal lattice (Fig. 3 (a)), underscoring pronounced conformational non-equivalence in the solid state. In comparison, alignment of the API conformers in Form K3 with the single crystallographically independent API molecule in Type H (mono-ACN solvate) further highlights substantial conformational divergence between the two forms. These differences persist despite both structures incorporating the same ACN solvate species, indicating that the observed conformational variability is not dictated solely by the identity of the guest molecule but rather reflects the broader adaptability of the host molecular framework (Fig. 3 (b)).

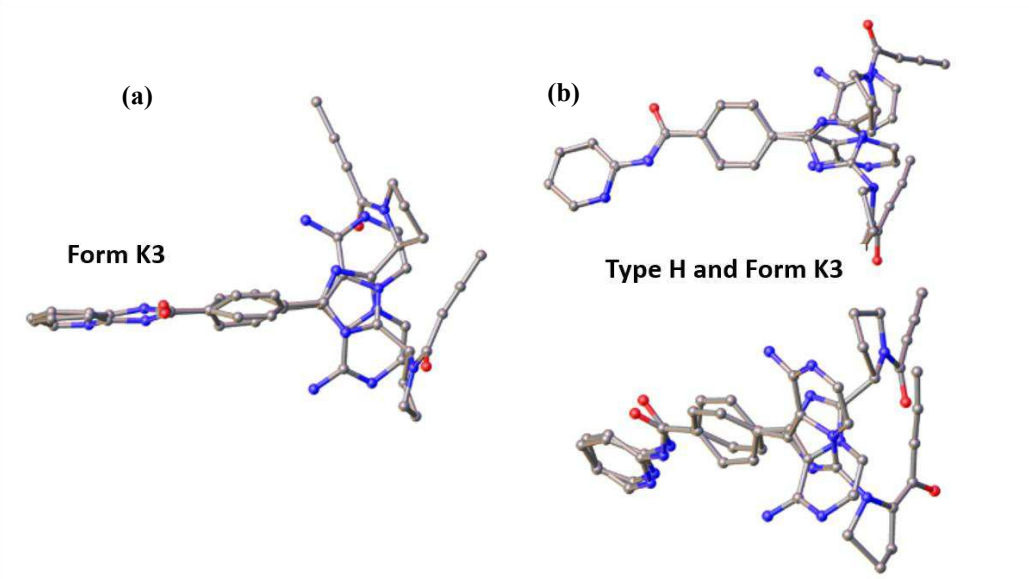



**Fig. 3** | Comparison of acalabrutinib molecular conformations in two acetonitrile-solvate structures. (a) Overlay of the two crystallographically independent acalabrutinib molecules in Form K3. (b) Overlay of the acalabrutinib molecule in Type H with the two crystallographically independent molecules in Form K3. Hydrogen atoms and acetonitrile molecules are omitted for clarity.

In addition to conformational flexibility, acalabrutinib possesses multiple hydrogen-bonding functionalities, including two hydrogen-bond donors and five acceptors (Fig. 2). This combination enables the formation of competing supramolecular synthons and diverse hydrogen-

bond motifs. Consistent with this, several distinct hydrogen-bonding motifs are observed across the resolved structures (Fig. 4). For example, in Form IV (anhydrate), adjacent acalabrutinib molecules are linked via a pair of N2–H2···N1 hydrogen bonds to form discrete dimers featuring an $R_2^2(8)$ hydrogen-bond motif, whereas another anhydrous Form I exhibits a directly interconnected three-dimensional hydrogen-bonding network. In Form K3, acalabrutinib molecules are connected through two different sets of $R_2^2(8)$ motifs to generate extended chain-like assemblies. In contrast, Type H features a *C*(13) chain motif formed through individual N6–H6···N1 hydrogen bonds. Collectively, these observations indicate that no single hydrogen-bonding arrangement dominates crystallization; rather, multiple competing intermolecular recognition patterns coexist within the solid-state landscape.

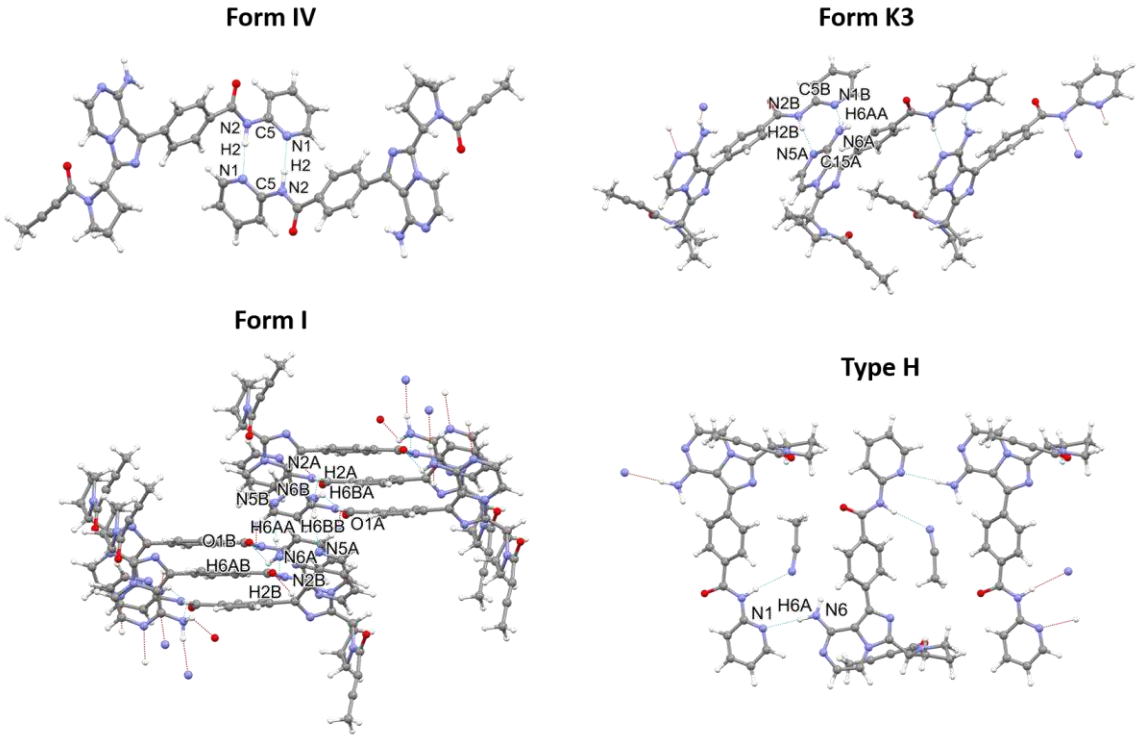



**Fig. 4** | Hydrogen bonding motifs observed in different crystal structures

Finally, the diversity of solvated crystal forms further highlights the structural adaptability of the system. Among the ten resolved structures, six are solvates, encompassing both channel-type and isolated-site solvates (Fig. 5). The crystal lattice accommodates chemically diverse guest molecules, including acetonitrile, acetylacetone, ethyl L-lactate, glycerol, and propylene glycol, indicating a flexible packing framework capable of adapting to guest-induced structural rearrangements. Solvent molecules play distinct structural roles across different forms: in some cases, acting as hydrogen-bond bridges that link adjacent acalabrutinib molecules, while in others participating only in terminal hydrogen-bond interactions without contributing to extended supramolecular connectivity. These differences highlight the context-dependent role of guest molecules in directing supramolecular organization and underscore their influence on the resulting crystal packing architecture.

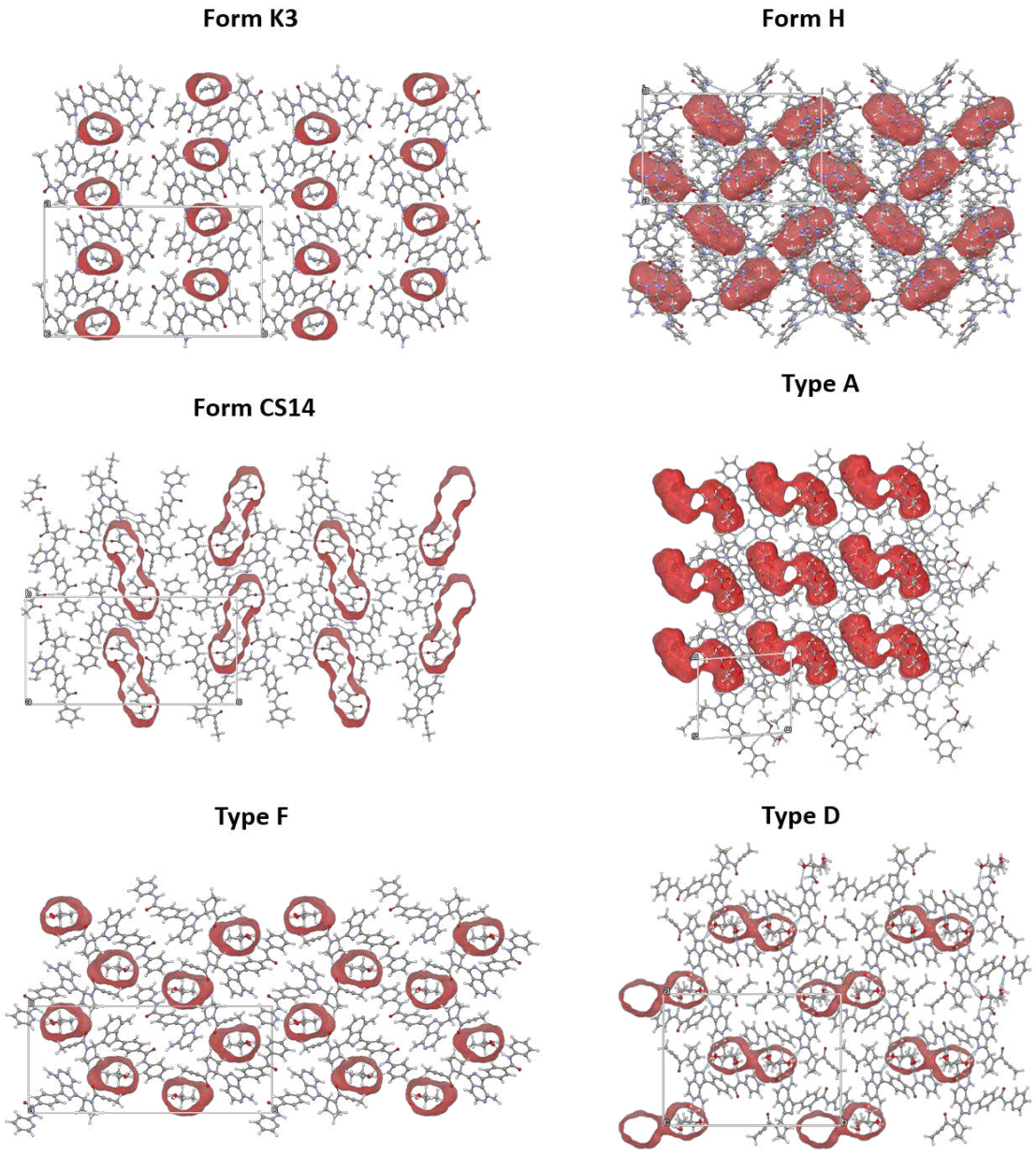



**Fig. 5** | Molecular packing structure diagrams for different solvates

## 3.6 Structural relationship between Form II and Form IV

Form II (trihydrate) and Form IV (anhydrate) exhibit a close structural relationship consistent with dehydration-associated conversion. The vacuum-dried Form II submission yielded Form IV by ED, while DVS showed that Form II dehydrates at low relative humidity. Together, these

observations support conversion during drying, transfer, or exposure to vacuum, although the conversion pathway was not directly observed.

Structural comparison shows that the molecular conformation of acalabrutinib is largely preserved between Forms II and IV, with no significant differences in the key torsional angles (Fig. 6). The principal structural differences instead involve the intermolecular interactions and lattice components. In the trihydrate, water molecules act as hydrogen-bond bridges within an extended three-dimensional network; in the anhydrous form, the absence of these water sites is accompanied by anisotropic contraction predominantly within the ab plane, while the packing arrangement along the crystallographic c axis remains largely conserved.

In Form IV, neighboring acalabrutinib molecules are brought into closer proximity and form discrete centrosymmetric dimers stabilized by paired intermolecular hydrogen bonds, generating characteristic hydrogen-bond motifs in the anhydrous form. These dimers assemble into a three-dimensional crystal-packing arrangement through slipped π–π stacking interactions and additional weak intermolecular contacts. The conservation of molecular conformation and related packing features provides a plausible structural basis for dehydration-associated conversion between Forms II and IV, but it does not establish a directly observed conversion mechanism.

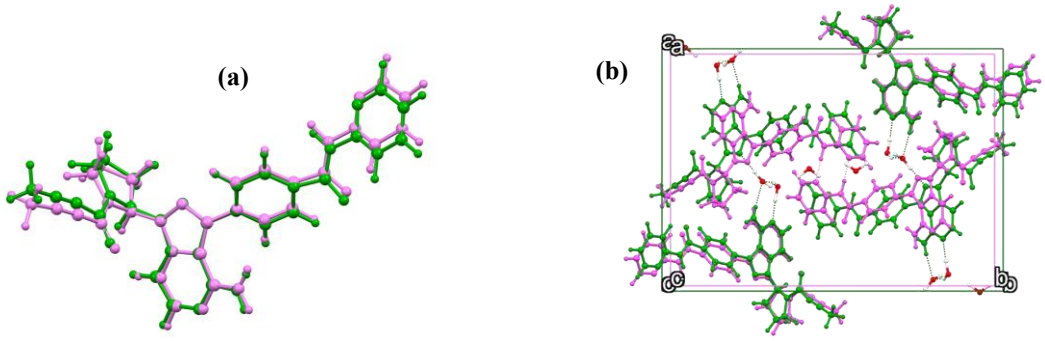



**Fig. 6** | (a) Conformational and (b) molecular packing structure comparison of the acalabrutinib Form II (trihydrate, green marked) and Form IV (anhydrate, magenta marked).

### 3.7 Absolute structure determination and absolute-configuration confirmation

Diffraction data collected using continuous-rotation ED are typically processed using the kinematical diffraction approximation, analogous to the approach used in SC-XRD. This kinematical approach is well validated and is the preferred workflow for routine, time-efficient structure determination. However, dynamical diffraction effects are present to some degree in ED experiments. Applying a dynamical treatment can improve crystallographic agreement and structural-model accuracy, with up to a fourfold reduction in difference Fourier-map noise reported in the literature. Because dynamical diffraction intensities are sensitive to absolute structure, dynamical refinement can distinguish between enantiomorphs from suitable ED datasets while also improving agreement factors and structural-model accuracy.[26,27]

The principal limitation of full dynamical refinement is its computational cost, which increases substantially with structural complexity and the number of refined parameters. For larger molecules such as acalabrutinib, this translates to substantially increased processing time and CPU requirements compared with kinematical refinement. A more tractable alternative is the "reduced" dynamical refinement approach, in which atomic positions and anisotropic displacement parameters (ADPs) are held fixed at values from the kinematical refinement, while only the specimen thickness and scale parameters are refined. This approach reduces the computation time to approximately 5–10 minutes per dataset on a standard laptop, with only a few refinement cycles required. [27]

For the purposes of the present study, full dynamical refinement was not required, as independent confirmation of the absolute configuration of acalabrutinib, a well-characterized clinical compound with known (S) stereochemistry, was not a primary objective, and it was not within scope to apply dynamical refinement to every structure determined. Nevertheless, to demonstrate the capability of ED for absolute configuration determination in the context of pharmaceutical solid-form screening, we applied the reduced dynamical refinement approach to one structure from this study.

Acalabrutinib contains one chiral center, and all crystal structures reported here were determined in chiral space groups (*P1, $P2_1$, $P2_12_12$, $P2_12_12_1$*, see Supplementary Information for details). The (S) absolute configuration of the chiral center is well established for acalabrutinib. The solvent molecule in Type F, the (S)-1,2-propanediol solvate, is itself chiral. This dataset was selected to demonstrate that ED, combined with reduced dynamical refinement, can unambiguously assign absolute configuration. This capability has significant implications beyond the present study: ED can in principle be used to confirm or determine absolute configuration for novel APIs or synthetic intermediates where chirality is unknown or requires independent verification.

The results of the reduced dynamical refinement for Type F are summarized in Table 7. Across all four datasets, the correct enantiomorph (S-API; S-solvate) consistently yielded lower $R_1$ and $wR_2$ values than the incorrect enantiomorph (R-API; R-solvate), confirming that enantiomorph 1 (S,S) represents the correct absolute structure assignment. Individual Z-scores ranged from 6.4 to 7.8 across the four datasets, all well above the 3σ threshold used to define statistical significance in absolute structure determination. The combined Z-score across all four datasets is 14.1, providing strong statistical support for the (S,S) absolute configuration assignment.

The same reduced dynamical refinement procedure could in principle be applied to all structures determined in this study. However, because the (S) absolute configuration of the API had been established and was independently confirmed for Type F, all other structures were modeled using the established (S) configuration of acalabrutinib in their respective Sohncke space groups.

**Table 7 | Results of reduced dynamical refinement on four ED datasets of Type F, the (S)-1,2-propanediol solvate.**

| | *Enantiomorph 1 (S-API; S-solvate)* | | *Enantiomorph 2 (R-API; R-solvate)* | | |
|---|---|---|---|---|---|
| ***Crystal*** | $R_1$**(obs)** | $wR_2$**(all)** | $R_1$**(obs)** | $wR_2$**(all)** | ***z*-score** |
| ***1*** | 12.14 | 23.48 | 14.13 | 27.30 | 6.530 |
| ***2*** | 15.89 | 29.34 | 17.93 | 32.96 | 7.822 |
| ***3*** | 13.81 | 28.37 | 15.68 | 30.64 | 6.417 |
| ***4*** | 13.23 | 26.00 | 14.96 | 29.29 | 7.313 |
| ***Combined*** | 14.11 | 27.20 | 16.02 | 30.53 | 14.079 |

# 4. Conclusions

This study evaluated whether ED can provide direct crystal-structure determination from crystalline materials generated through routine pharmaceutical solid-form workflows. The ten selected acalabrutinib forms encompassed anhydrates, hydrates, and solvates and were not selected based on apparent crystallinity, morphology, or anticipated ED performance. Without purpose-grown single crystals or crystal-morphology optimization, ED successfully determined crystal structures from all ten submitted samples. Nine structures corresponded to the nine selected solid forms, whereas the sample submitted as Form K1 yielded Form II following solid-form conversion. The study therefore achieved crystal-structure determination for all ten samples and confirmation of the intended solid form for nine.

Sample preparation and handling strongly affected both diffraction quality and preservation of the intended solid form. For several labile hydrates and solvates, vacuum-dried or room-temperature air-dried preparations produced poorer or less complete structural results, and the vacuum-dried Form II sample yielded the anhydrous Form IV. Among the combinations evaluated, mother-liquor preservation combined with cryogenic preparation most consistently supported structure determination for labile forms. This combined approach provides a practical, stability-guided strategy for labile hydrates and solvates, although it was not required for every form.

ED also resolved ambiguities in water or solvent content and provided direct information on molecular conformation, crystal packing, hydrogen-bonding networks, and individual crystalline forms within mixtures. Reduced dynamical refinement of Type F further confirmed the established absolute configurations of the API and chiral solvate, demonstrating the applicability of ED to configurational assignment when suitable data are available.

Together, these findings establish a systematic single-compound benchmark supporting the incorporation of MicroED into routine pharmaceutical solid-form workflows. ED enables direct crystal-structure determination from crystalline powders without purpose-grown single crystals, and mother-liquor preservation combined with cryogenic preparation can extend its applicability to labile forms that may not withstand drying or room-temperature transfer. When integrated with conventional characterization, ED can make solid-form identification more definitive and provide a more complete understanding of a compound's solid-form landscape. This combined approach could bring pharmaceutical solid-state science closer to a long-standing goal: obtaining direct crystal-structure information for every crystalline form encountered during routine screening and subsequent preparation.

# 5. Methods

## 5.1 Selection and preparation of solid forms

Ten distinct acalabrutinib crystalline forms were included to provide a comparatively large and diverse test set for a single compound. Eight forms were initially selected based on the availability of existing material in stock, and two additional forms were selected and re-prepared using routine crystallization procedures derived from the polymorph-screening campaign to bring the set to ten. The set deliberately encompassed anhydrates, hydrates, and solvates. Subject to sample availability, set size, and solid-form diversity, the forms were selected without regard to apparent crystallinity, crystal dimensions, morphology, or anticipated diffraction quality. The evaluated materials therefore comprised existing samples from routine polymorph screening and

samples obtained through routine re-preparation or scale-up. No crystallization experiments specifically targeting single-crystal growth, crystal morphology, or ED suitability were performed. Detailed preparation histories and sample identifiers are provided in Supplementary Table 1.

## 5.2 Conventional solid-state characterization

XRPD patterns were collected using a Bruker D8 Advance diffractometer with Cu Kα radiation (λ = 1.5406 Å) over a 2θ range of 4–40°, with a step size of 0.02° and a scanning rate of 0.3 s per step. Samples were placed on a low-background silicon holder before measurement. Differential scanning calorimetry was performed using a TA Instruments Discovery DSC2500. Approximately 2–5 mg of sample was heated from 25 to 300 °C at 10 °C $min^{-1}$ under nitrogen. Thermogravimetric analysis was performed using a TA Instruments Discovery TGA5500. Approximately 2–5 mg of sample was heated from room temperature to 350 °C at 10 °C $min^{-1}$ under nitrogen.

Dynamic vapor sorption measurements were performed using a Surface Measurement Systems DVS Intrinsic. Approximately 5–20 mg of sample was analyzed at 25 °C over a relative humidity range of 0–95%. Relative humidity was increased in 10% increments, and equilibrium was defined as a mass change of less than 0.002% per minute over 10 min. Variable-temperature XRPD measurements were performed using a PANalytical Empyrean diffractometer with Cu Kα radiation (λ = 1.540598 Å). Samples were scanned over a 2θ range of 3–40° with a step size of 0.0167° at selected temperatures during heating from 30 to 190 °C and were equilibrated at each temperature before data collection. $^{1}$H NMR spectra were recorded on a Bruker 400 MHz spectrometer at 25 °C using approximately 5 mg of sample dissolved in an appropriate deuterated solvent (DMSO-$d_6$).

## 5.3 ED sample preparation and data collection

For cryogenic preparation, a drop of mother-liquor suspension or a small amount of moist solid was placed at room temperature on a 3 mm-diameter copper TEM grid covered with lacey carbon film. Excess liquid was blotted with filter paper at room temperature. The loaded grid was then plunge-cooled in liquid nitrogen and transferred under cryogenic conditions into the diffractometer using an inert transfer chamber. The interval between plunge cooling and transfer was kept below 30 s to maintain the sample at low temperature and minimize crystalline-form changes during handling. Thus, the sample was loaded onto the grid at room temperature rather than applied directly to a cryogenically cooled grid. For room-temperature preparation of dried powders, the powder was gently dispersed on the TEM grid and transferred into the electron diffractometer at room temperature. The sample was then cooled inside the diffractometer for approximately 30 min before measurement.

Data were collected using three-dimensional electron diffraction (3D ED), commonly termed microcrystal electron diffraction (MicroED), at 123(2) K using an ELDICO ED-1 electron diffractometer equipped with a $LaB_6$ electron source and a hybrid-pixel Dectris QUADRO detector. The electron wavelength was 0.02851 Å, and continuous-rotation experiments were performed for all samples. For manual data collection, the total rotation range was generally 60–110°, with 1° slicing and an exposure time of 1 s per degree. For automated measurements, the total rotation range was 30°, with 1° slicing and an exposure time of 1 s per degree, and a larger number of datasets were collected.

## 5.4 ED data processing, structure solution, and refinement

Data were integrated using DIALS 3.25.0 without absorption correction. Multiple datasets were merged to improve completeness and redundancy. Structures were solved by intrinsic phasing using SHELXT 2018/2 and refined by full-matrix least squares against $F^2$ using SHELXL-2019/2.

Non-hydrogen atoms were refined with anisotropic displacement parameters. C-bound hydrogen atoms were refined with isotropic displacement parameters; selected coordinates were refined freely, whereas others were placed in calculated positions using a riding model. Uiso was constrained to 1.5 times Ueq of the pivot atom for terminal $sp^3$ carbon atoms and 1.2 times Ueq for other carbon atoms. Neutron-diffraction bond distances were used for C–H and N–H bonds. CIF files were generated using FinalCif or the CIF generator in Olex2. Software references and additional crystallographic details are provided in the Supplementary Information.

### 5.5 Reduced dynamical refinement

Data used for reduced dynamical refinement were processed using PETS2. After unit-cell determination, frames were integrated, corrected for pattern orientation and beam position, and merged into overlapping virtual frames with a tilt range of 3° and an offset of 2° between frames. Dynamical refinement was performed using JANA2020 with the structure obtained by kinematical refinement as the starting structural model. Least-squares refinements minimized $\Sigma w(I_{obs} - I_{calc})^2$ based on dynamical diffraction intensities and assumed uniform crystal thickness. Atomic positions and anisotropic displacement parameters from the kinematical refinement were held fixed, whereas crystal-thickness and scale parameters were refined. Results were validated using the Z-score method described in the Supplementary Information.

## Data availability

The crystallographic data generated in this study have been deposited with the Cambridge Crystallographic Data Centre under deposition numbers 2548852, 2548853, 2554539, 2554541, 2548854, 2548858, 2548855, 2548857, 2554544, and 2548856. These data are available free of charge from the CCDC at https://www.ccdc.cam.ac.uk/structures/. The additional data supporting the findings of this study are provided in the Article and its Supplementary Information.

## References


1. Bernstein, J. *Polymorphism in Molecular Crystals*, 2nd edn (Oxford Univ. Press, Oxford, 2020).
2. Brittain, H. G. *Polymorphism in Pharmaceutical Solids*, 2nd edn (Informa Healthcare, New York, 2009).
3. Hilfiker, R. & von Raumer, M. (eds) *Polymorphism in the Pharmaceutical Industry: Solid Form and Drug Development* (Wiley-VCH, Weinheim, 2018).
4. International Council for Harmonisation of Technical Requirements for Pharmaceuticals for Human Use. Specifications: Test Procedures and Acceptance Criteria for New Drug Substances and New Drug Products: Chemical Substances (Q6A). (1999).
5. US Food and Drug Administration. ANDAs: Pharmaceutical Solid Polymorphism–Chemistry, Manufacturing, and Controls Information: Guidance for Industry (2007).
6. Giacovazzo, C. et al. *Fundamentals of Crystallography*, 3rd edn (Oxford Univ. Press, Oxford, 2011).
7. Karothu, D. P. et al. The elusive structure of levocetirizine dihydrochloride determined by electron diffraction. *Angew. Chem. Int. Ed.* **62,** e202303761 (2023).
8. Jones, C. G. et al. The cryoEM method MicroED as a powerful tool for small molecule structure determination. *ACS Cent. Sci.* **4,** 1587–1592 (2018).
9. Chambi, J. T., Fandaruff, C. & Cuffini, S. L. Identification and quantification techniques of polymorphic forms–A review. *J. Pharm. Biomed. Anal.* **242,** 116038 (2024).
10. Giron, D. Thermal analysis and calorimetric methods in the characterization of polymorphs and solvates. *Thermochim. Acta* **248,** 1–59 (1995).
11. Grobelny, P., Mukherjee, A. & Desiraju, G. R. Polymorphs and hydrates of Etoricoxib. *CrystEngComm* **14,** 5785–5794 (2012).

12. Gruene, T. et al. Rapid structure determination of microcrystalline molecular compounds using electron diffraction. *Angew. Chem. Int. Ed.* **57,** 16313–16317 (2018).
13. Gemmi, M. et al. 3D electron diffraction: the nanocrystallography revolution. *ACS Cent. Sci.* **5,** 1315–1329 (2019).
14. Gruene, T., Holstein, J. J., Clever, G. H. & Keppler, B. Establishing electron diffraction in chemical crystallography. *Nat. Rev. Chem.* **5,** 660–668 (2021).
15. Simoncic, P. et al. Electron crystallography and dedicated electron-diffraction instrumentation. *Acta Crystallogr. E* **79,** 410–422 (2023).
16. Center for Drug Evaluation, National Medical Products Administration. *Technical Guideline for the Study of Polymorphism of Innovative Chemical Drugs (For Trial Implementation)*. https://www.cde.org.cn/main/news/viewInfoCommon/624ddccf6e11f58f63b8ca84da210efd (2026).
17. Ungur, D. T. et al. Crystal structure of febuxostat marketed polymorph determined by electron diffraction and reinforced by X-ray crystallography. *CrystEngComm* **26,** 4295–4304 (2024).
18. Sieger, P., Werthmann, U. & Saouane, S. The polymorph landscape of dabigatran etexilate mesylate: Taking the challenge to bring a metastable polymorph to market. *Eur. J. Pharm. Sci.* **186,** 106447 (2023).
19. Bruhn, J. F. *et al.* Small molecule microcrystal electron diffraction for the pharmaceutical industry–lessons learned from examining over fifty samples. *Front. Mol. Biosci.* **8,** 648603 (2021).
20. Danelius, E., Patel, K., Gonzalez, B. & Gonen, T. MicroED in drug discovery. *Curr. Opin. Struct. Biol.* **79,** 102549 (2023).
21. Nannenga, B. L. & Gonen, T. The cryo-EM method microcrystal electron diffraction (MicroED). *Nat. Methods* **16,** 369–379 (2019).

22. Acehan, D. et al. Reaching the potential of electron diffraction. *Cell Rep. Phys. Sci.* **5,** 102007 (2024).
23. U.S. Food and Drug Administration. CALQUENCE (acalabrutinib) capsules, for oral use: Prescribing Information (2017).
24. Blatter, F. et al. Crystal forms of (S)-4-(8-amino-3-(1-(but-2-ynoyl)pyrrolidin-2-yl)imidazo[1,5-a]pyrazin-1-yl)-N-(pyridin-2-yl)benzamide. US Patent 9,796,721 B2 (2017).
25. Unge, J., Nannenga, B. L., Oliver, A. G. & Gonen, T. Standards for MicroED. *Acta Crystallogr. C Struct Chem*. **81,** 376-390 (2025).
26. Klar, P. B. et al. Accurate structure models and absolute configuration determination using dynamical effects in continuous-rotation 3D electron diffraction data. *Nat. Chem.* **15,** 848–855 (2023).
27. Klar, P. B., Brázda, P., Krysiak, Y., Klementová, M. & Palatinus, L. Absolute configuration directly determined from 3D electron diffraction data. *Acta Crystallogr. A Found. Adv.* **77,** C210 (2021).

## Acknowledgements

This work was funded by Crystal Pharmatech and Eldico Scientific AG. The authors thank Suzhou PengXu Pharmatech Co., Ltd. for providing the starting materials used in the polymorph screening, scale-up, and sample preparation experiments.

## Author contributions

A.M.C. conceived the study, designed the benchmark, and initiated the collaboration between Crystal Pharmatech and Eldico Scientific. Y.C. led the experimental program at Crystal Pharmatech, coordinated work with Eldico Scientific, and drafted the sections on polymorph screening, conventional solid-state characterization, and comparison of conventional and ED-derived assignments. Y.L., C.H. and J.Q. performed polymorph screening, conventional solid-state characterization (XRPD, VT-XRPD, TGA, DSC, DVS and $^{1}$H NMR), and preparation of samples for ED analysis. Y.X. interpreted the ED-derived structures and performed comparative analyses of molecular conformation, hydrogen-bonding motifs and crystal packing. L.M. oversaw the experimental program at Crystal Pharmatech. G.S., C.J. and J.M. performed ED grid preparation, data collection and processing, and structure solution and refinement, including reduced dynamical refinement. G.S.-Q. directed the ED work at Eldico Scientific and drafted the sections on ED methodology, structure determination and structural interpretation. H.Z. provided technical guidance and critically reviewed the manuscript. R.W. contributed to interpretation of the solid-state characterization data and critically reviewed the manuscript. A.M.C. and G.S.-Q. supervised the study. All authors reviewed, revised and approved the manuscript.

## Competing interests

G.S.-Q., G.S., C.J. and J.M. are employees of Eldico Scientific AG, which manufactures and commercializes the ELDICO ED-1 electron diffractometer used in this study; G.S.-Q. and G.S. are founders and shareholders of the company. Y.C., Y.X., Y.L., C.H., J.Q., L.M., R.W. and A.M.C. are employees of Crystal Pharmatech. H.Z. serves as Dean of the Institute of Frontier Solid-State Chemistry at Crystal Pharmatech. Crystal Pharmatech commercially provides pharmaceutical solid-state research services, including polymorph screening, solid-form characterization and ED-based crystal-structure determination; R.W. and A.M.C. are co-founders and shareholders of Crystal Pharmatech. This study was funded by Crystal Pharmatech and Eldico Scientific AG.

## Supplementary Files

This is a list of supplementary files associated with this preprint. Click to download.

- SupplementaryInformation.docx